FIRST-PRINCIPLES APPROACH TO THE MECHANICAL PROPERTIES OF Al_2CuX ALLOYS

by

Wen-Yu QIAN[a] and Yu CHEN[b*]

[a]School of Civil Engineering, Inner Mongolia University of Technology, Hohhot, China
[b]College of Science, Inner Mongolia University of Technology, Hohhot, China

Original scientific paper
https://doi.org/10.2298/TSCI2503927Q

The mechanical properties of Al_2CuX (X = Y, Zr, Nb, Mo, Tc, Ru, Rh, Pd, Ag, Cd) alloys have been studied using the first-principles calculation. By analyzing the mechanical stability, it was found that Al_2CuRh and Al_2CuCd are mechanically unstable, and Al_2CuPd and Al_2CuAg do not satisfy the Voigt-Reuss-Hill theory. Therefore, in this work only studies the mechanical properties of Al_2CuX (X = Y, Zr, Nb, Mo, Tc, Ru), we found the bulk modulus, shear modulus, Young's modulus and Vickers hardness and Pugh's modulus ratio of Al_2CuX are increases, while the Poisson's ratio decreases. In summary, studying the mechanical properties of Al_2CuX provides more options for optimal design and advanced applications of Al alloys.

Key words: *fist-principles, mechanical stability, elastic modulus, alloys, vickers hardness*

Instructions

Al alloys were started and put into commercial applications in the 1970's, and research on Al alloys has continued in recent years. The main purpose of research on Al alloys is to enhance their mechanical properties by improving strength, hardness and ductility. The Al alloys have evolved from the earliest dual alloy to the study of ternary alloy or even multiple alloy [1-3], and the alloy is no longer single. Common metal elements, *e.g.*, Fe, Cr, Ni, Ti, Cu, and Zn, can be used as the composition of Al alloys [4-8].

The mechanical properties of the Al-Cu based alloy formed after adding Cu to Al, *e.g.*, hardness, ductility and strength, have been improved [9-11]. Adding other elements to the Al-Cu alloys, such as rare earth and alkaline metals [12-17], higher Yang's modulus, higher hear modulus and higher ductility are predicted. A large number of studies have shown that alloy diversification can significantly improve the comprehensive properties of Al alloy, and the added elements are mainly Li, Mg, and rare earth [17-20].

In this paper, the mechanical properties of Al_2CuX (X = Y, Zr, Nb, Mo, Tc, Ru, Rh, Pd, Ag, Cd) alloy are investigated by the first principles.

Computational methods

In this work, the first-principles calculation is used to study the properties of Al_2CuX (X = Y, Zr, Nb, Mo, Tc, Ru, Rh, Pd, Ag, Cd) by the density functional theory (DFT)

* Corresponding author, e-mail: chenyu@imut.edu.cn

using a plane-wave pseudopotential method as implemented in the Cambridge Sequential Total Energy Package (CASTEP) code [20-22]. The Generalized Gradient Approximation (GGA) within the Perdew, Burke, and Ernzerhof (PBE) scheme is used to obtain the exchange correlation potential. In order to ensure the accuracy of the calculation, we use the plane-wave energy cutoff of 600 eV and the Brillouin zone sampling mesh parameters for the k-point set of 6×6×6. The other parameters use the default settings of ultra-fine accuracy.

In this work, Al_3Cu compounds were obtained by substituting one vertex Al atom with one Cu atom in a 1×1×1 Al_4 supercell models as shown in fig. 1(a). The supercell contains three Al atoms and one Cu atom, and the supercells were used to study the mechanical properties of Al_3Cu. The Al_2CuX compounds were obtained by replacing one Al atom with one X atom in an Al_3Cu supercell models as shown in fig. 1(b). The supercell contains two Al atoms, one Cu atom and one X atom, and the supercells were used to study the mechanical properties of Al_2CuX.

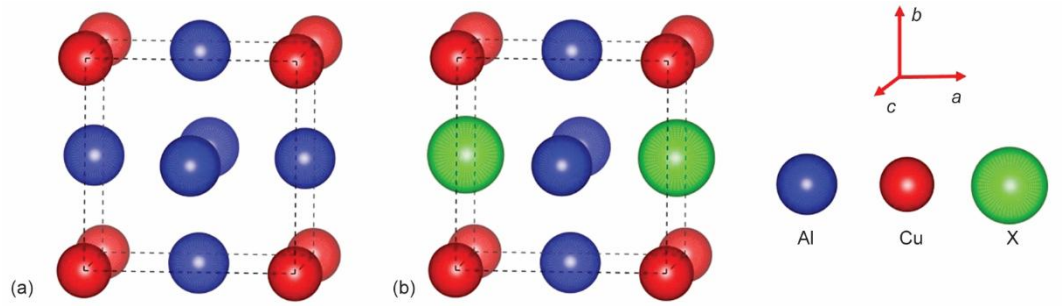

Figure 1. (a) The supercell models of Al_3Cu and (b) the supercell models of Al_2CuX

Results and discussion

Elastic constants and mechanical stability

Elastic constants of crystals provide a link between mechanical and dynamic behavior. They also provide important information about the elastic response of a crystal to external pressure. Elastic constants are important parameters for describing the mechanical properties of solids. This elastic matrix has a size of 6×6 and is symmetric. The higher the symmetry of the crystal, the fewer independent elastic constants there are. The maximum number of independent elastic stiffness constants is 21. The elastic constants, C_{ij}, for the orthorhombic Al_2CuX supercell obtained by the GGA method. According to the elastic constants, it is found that Al_2CuX belongs to orthorhombic crystal. The mechanical stabilities of the crystal structure under isotropic pressure can be determined by the criteria of independent C_{ij}. For an orthorhombic crystal, there are independent components as shown in the following equation [23, 24]:

$$\begin{gathered} C_{ii} > 0 \\ C_{11} + C_{22} - 2C_{12} > 0 \\ C_{11} + C_{33} - 2C_{13} > 0 \\ C_{22} + C_{33} - 2C_{23} > 0 \\ C_{11} + C_{22} + C_{33} + 2(C_{12} + C_{13} + C_{23}) > 0 \end{gathered} \tag{1}$$

According to the criteria, all Al_2CuX except Al_2CuRh and Al_2CuCd are mechanically stable at ambient pressure. Therefore, only the mechanical properties of Al_2CuX (X = Y, Zr, Nb, Mo, Tc, Ru, Pd, Ag) will be studied in the following.

Elastic modulus

The elastic modulus of polycrystalline is related to the elastic constants of single crystal. In general, elastic properties of polycrystalline have greater practical significance than those of single crystal. Polycrystalline elastic properties are properties of bulk modulus, *B*, shear modulus, *G*, Young's modulus, *E*, and Poisson's ratio. There are two models for evaluating the modulus: the Voigt method and the Reuss method, which provide the upper and lower limits of the polycrystalline elastic modulus, respectively. For different crystalline systems, the bulk and shear moduli according to Voigt can be expressed [25, 26]:

$$B_{\mathrm{v}} = \frac{C_{11} + C_{22} + C_{33} + 2(C_{12} + C_{13} + C_{23})}{9} \tag{2}$$

$$G_{\mathrm{v}} = \frac{C_{11} + C_{22} + C_{33} - C_{12} - C_{13} - C_{23}}{15} + \frac{C_{44} + C_{55} + C_{66}}{5} \tag{3}$$

The the bulk and shear moduli in Reuss opinon are:

$$B_{\mathrm{R}} = \frac{1}{S_{11} + S_{22} + S_{33} + 2(S_{12} + S_{13} + S_{23})} \tag{4}$$

$$G_{\mathrm{R}} = \frac{15}{4(S_{11} + S_{22} + S_{33}) + 3(S_{44} + S_{55} + S_{66}) - 4(S_{12} + S_{13} + S_{23})} \tag{5}$$

Bulk modulus and shear modulus can be obtained using the Voigt-Reuss-Hill method. The arithmetic mean of the Voigt and Reuss limits is known as the Voigt-Reuss-Hill mean, which is considered the best estimate of the theoretical value of the polycrystalline elastic modulus:

$$B = \frac{B_{\mathrm{V}} + B_{\mathrm{R}}}{2} \tag{6}$$

$$G = \frac{G_{\mathrm{V}} + G_{\mathrm{R}}}{2} \tag{7}$$

The Young's modulus and Poisson's ratio can be computed based on the previous values by:

$$E = \frac{9BG}{3B + G} \tag{8}$$

$$\mu = \frac{3B - 2G}{6B + 2G} \tag{9}$$

The *B*, *G*, *E* and μ of Al_2CuX are calculated according to eqs. (2)-(9). The calculation results are shown in fig. 2. The green dashed line represents modulus of Al_3Cu.

According to the Voigt-Reuss-Hill theory, for Al_2CuPd and Al_2CuAg, their B_V is smaller than B_R, obviously these experimental data are unacceptable, similarly, their G_V is smaller than G_R, and these experimental data are also unacceptable. Therefore, in this work only mechanical properties of Al_2CuX (X = Y, Zr, Nb, Mo, Tc, Ru) are studied.

The bulk modulus B of Al_2CuX is illustrated in fig. 2(a). Following the introduction of X into Al_3Cu, the bulk modulus B of Al_2CuY is diminished, while the bulk modulus B of other Al_2CuX is augmented. The bulk modulus of Al_2CuRu is the greatest (162.05 GPa) and the bulk modulus of Al_2CuY is the least (74.36 GPa).

The shear modulus G of Al_2CuX is shown in fig. 2(b). After doping X into Al_3Cu, the shear modulus G of all Al_2CuX is increased. The shear modulus of Al_2CuNb is the largest (92.73 GPa) and the shear modulus of Al_2CuZr is the smallest (51.72 GPa).

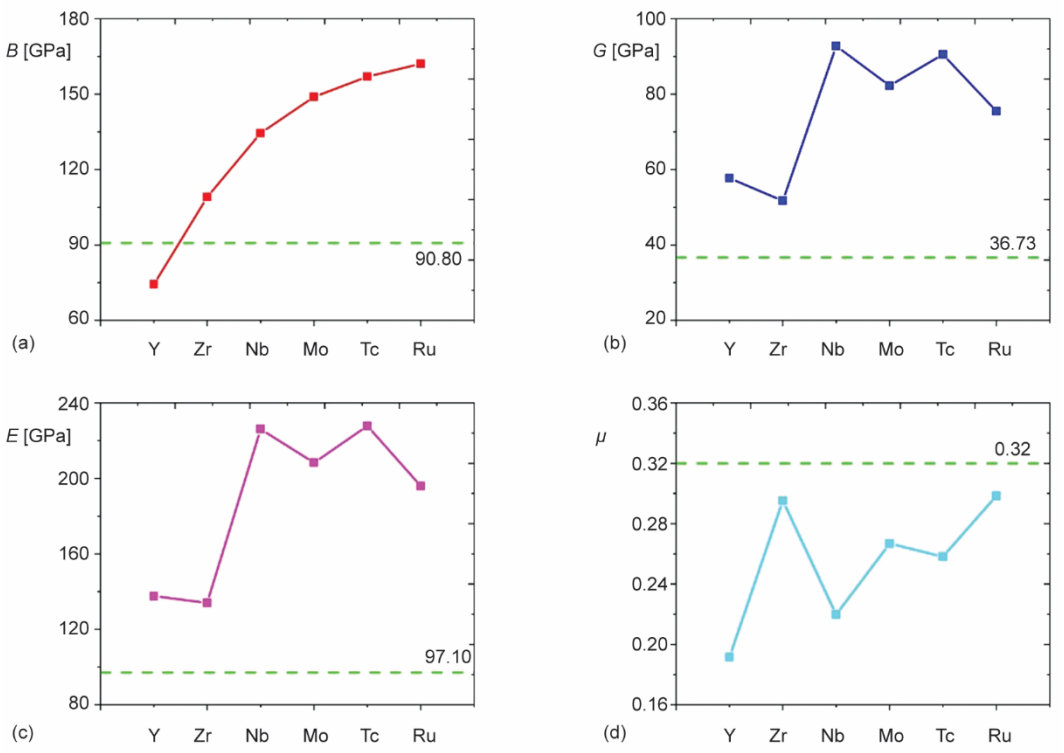

Figure 2. (a) The bulk modulus of Al_2CuX, (b) the shear modulus of Al_2CuX, (c) the Young's modulus of Al_2CuX, and (d) the Poisson's ration of Al_2CuX

The Young's modulus E of Al_2CuX is shown in fig. 2(c). Following the introduction of X into Al_3Cu, the Young's modulus E of all Al_2CuX is elevated. The Young's modulus of Al_2CuTc is the greatest (227.77 GPa) and that of Al_2CuZr is the smallest (133.99 GPa).

The Poisson's ratio of Al_2CuX is illustrated in fig. 2(d). Following the doping of X into Al_3Cu, the Poisson's ratio of all Al_2CuX is observed to decrease. The Poisson's ratio of Al_2CuZr and Al_2CuRu is found to be the largest (0.30), while that of Al_2CuY is the smallest (0.19).

Vickers hardness and ductility

The hardness of a material is defined as its intrinsic resistance to deformation when a force is applied. At present, a formal theoretical definition of hardness remains a challenge for material scientists. The hardness of a material is related to its elastic and plastic properties. Some semi-empirical models have been developed to predict the hardness of materials. Zhou *et al.* [27] proposed a model to predict the hardness of polycrystalline materials and bulk metallic glasses based on the Pugh's modulus ratio ($k = G/B$) and the shear modulus:

$$H_V = 1.887k^{1.171}G^{0.591} \tag{10}$$

where H_V denotes the Vickers hardness.

The ratio of B/G can be employed to estimate the ductility or brittleness of materials [28, 29], given that a high (low) value is correlated with ductility (brittleness). The critical value is approximately 1.75:

$$D = \frac{B}{G} \tag{11}$$

The H_V and B/G of Al_2CuX are calculated according to eqs. (10) and (11). The calculation results are shown in fig. 3. The green dashed line represents the Hv and B/G of Al_3Cu.

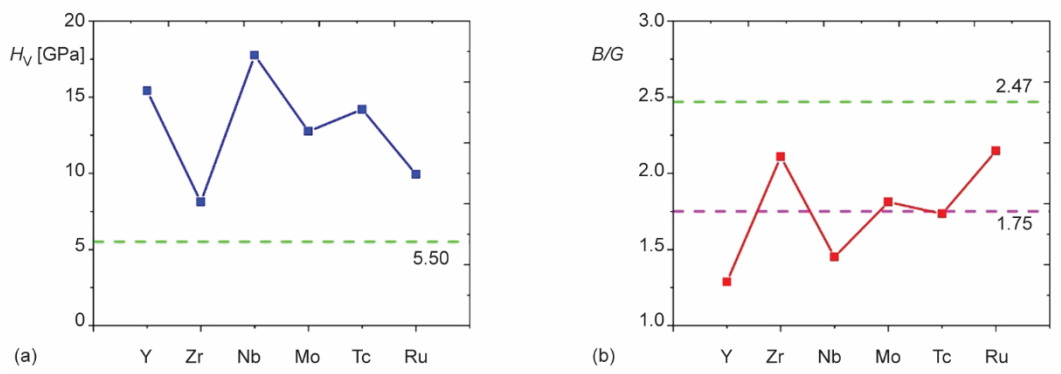

Figure 3. (a) The H_V of Al_2CuX and (b) the B/G of Al_2CuX

The Vickers hardness H_V of Al_2CuX is illustrated in fig. 3(a). Following the introduction of X into Al_3Cu, the Vickers hardness of all Al_2CuX compounds is observed to increase. The Vickers hardness of Al_2CuNb is the greatest (17.15 GPa), while that of Al_2CuZr is the lowest (8.11 GPa).

The B/G ratio of Al_2CuX is depicted in fig. 3(b). Following the doping of X into Al_3Cu, the ductility of all Al_2CuX was found to decrease. The ductility of Al_2CuRu is the greatest (2.15), while that of Al_2CuY is the least (1.29). The Al_2CuZr, Al_2CuMo, and Al_2CuRu alloys exhibit enhanced ductility, with B/G values exceeding 1.75. The Al_2CuY, Al_2CuNb, and Al_2CuTc alloys exhibit greater brittleness, with B/G values below 1.75.

Elastic anisotropy

A number of techniques have been devised to estimate the elastic anisotropy of a compound. The bulk modulus anisotropy, A_B, and shear modulus anisotropy, A_G, for a crystal with orthorhombic symmetry can be determined using the following equations [26]:

$$A_B = \frac{B_V - B_R}{B_V + B_R}$$
$$A_G = \frac{G_V - G_R}{G_V + G_R} \tag{12}$$

The zero value of the anisotropic index (A_B, A_G) indicates that the crystal is isotropic. A high value of the anisotropic index (A_B, A_G) indicates that the crystal structure exhibits highly anisotropic elastic properties. The A_B and A_G values for Al_2CuX are calculated in accordance with eq. (12). The results of the calculations are presented in fig. 4. The green dashed line represents the A_B and A_G of Al_3Cu.

The bulk modulus anisotropy (A_B) of Al_2CuX is illustrated in fig. 4(a). Following the introduction of X into Al_3Cu, the bulk modulus anisotropy (A_B) of Al_2CuX is observed to increase slightly. The bulk modulus anisotropy of Al_2CuX is notably minimal, approaching zero. The bulk modulus anisotropy (A_B) of Al_2CuY is the most pronounced (0.29%).

The A_G of Al_2CuX is depicted in fig. 4(b). Following the introduction of X into Al_3Cu, the shear modulus anisotropy of Al_2CuX is observed to decrease, with the exception of Al_2CuRu. The shear modulus anisotropy of Al_2CuRu is the largest (18.97%), while that of Al_2CuNb is the smallest (0.73%).

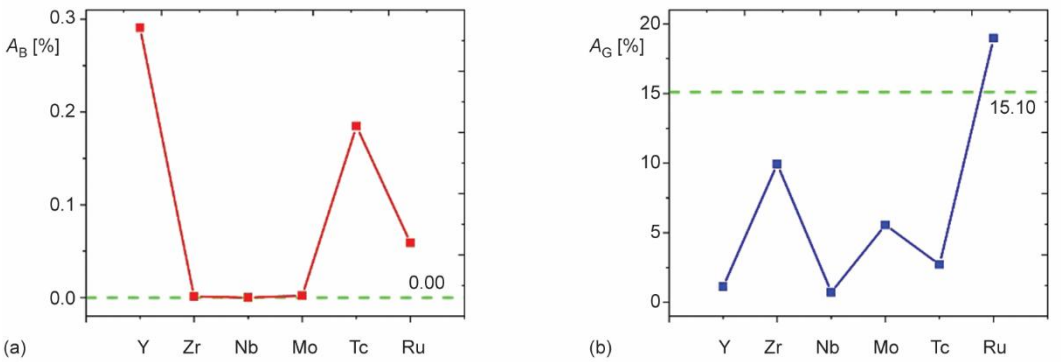

Figure 4. (a) The bulk modulus anisotropy factors of Al_2CuX, (b) the shear modulus anisotropy factors of Al_2CuX, and (c) the universal elastic anisotropy factors of Al_2CuX

Conclusion

This work, based on first-principles calculations, studies the mechanical properties of Al_2CuX (X = Y, Zr, Nb, Mo, Tc, Ru, Rh, Pd, Ag, Cd) crystals in the orthorhombic phase. Our analysis reveals that Al_2CuRh and Al_2CuCd are mechanically unstable. The Voigt-Reuss-Hill theory shows that for Al_2CuPd and Al_2CuAg, their B_V is smaller than B_R, and their G_V is less than G_R. These experimental data are therefore unacceptable. This work therefore only studies the mechanical properties of Al_2CuX (X = Y, Zr, Nb, Mo, Tc, Ru). We have found

that the bulk modules, shear modulus, Young's modulus, and Vickers hardness of Al_2CuX increase, while the Poisson's ratio and *B*/*G* decrease. The elastic anisotropy changes are not obvious. In short, doping with 4d transition metals has a positive effect on the improvement of the elastic modulus and Vickers hardness of Al_2CuX alloy. However, the decrease in ductility limits its application. The comprehensive analysis of the mechanical properties of the Al_2CuX alloy has demonstrated that it is a high-quality alloy with significant potential for engineering applications. The results of this paper provide a solid theoretical basis for the application of the Al_2CuX alloy. The results also suggest a promising approach to design nanofibers [30-34] using the first-principles, the designed electrospun nanofibers can be used for gas purification [35], and wearable sensors [36].

Acknowledgment

The research work is supported by the Basic Scientific Research Expenses Program of Universities directly under Inner Mongolia Autonomous Region (JY20220213).

References

[1] Wang, S. Q., *et al.*, First-Principles Study of the Formation of Guinier-Preston Zones in Al-Cu Alloys, *Scripta Materialia, 51* (2004), 7, pp. 665-669
[2] Wang, J., *et al.*, First-Principles Growth Kinetics and Morphological Evolution of Cu Nanoscale Particles in Al, *Acta Materialia, 53* (2005), 9, pp. 2759-2764
[3] Sun, D., *et al.*, First-Principles Calculation on the Thermodynamic and Elastic Properties of Precipitations in Al-Cu Alloys, *Superlattices and Microstructures, 100* (2016), Dec., pp. 112-119
[4] Wang, A., *et al.*, First-Principles Study of Binary Special Quasirandom Structures for the Al-Cu, Al-Si, Cu-Si, and Mg-Si Systems, *Calphad, 33* (2009), 4, pp. 769-773
[5] Yang, C. D., *et al.*, Study on Mechanical Behavior and Electronic Structures of Al-Cu Intermetallic Compounds Based on First-Principles Calculations, *Solid State Communications, 151* (2011), 18, pp. 1270-1274
[6] Zhang, J., *et al.*, Structural, Elastic and Electronic Properties of θ (Al_2Cu) and S (Al_2CuMg) Strengthening Precipitates in Al-Cu-Mg Series Alloys: First-Principles Calculations, *Solid State Communications, 152* (2012), 23, pp. 2100-2104
[7] Gao, Q., *et al.*, First-Principles Calculations of Finite-Temperature Thermodynamic Properties of Binary Solid Solutions in the Al-Cu-Mg System, *Calphad, 47* (2014), Dec., pp. 196-210
[8] Ren, M., *et al.*, Transition Metal Atoms (Fe, Co, Ni, Cu, Zn) Doped RuIr Surface for the Hydrogen Evolution Reaction: A first-Principles Study, *Applied Surface Science, 556* (2021), 149801
[9] Choi, G., *et al.*, Study on Thermal Conductivity and Electrical Resistivity of Al-Cu Alloys Obtained by Boltzmann Transport Equation and First-Principles Simulation: Semi-Empirical Approach, *Journal of Alloys and Compounds, 727* (2017), Dec., pp. 1237-1242
[10] Liu, H., *et al.*, Precipitation during High Temperature Aging of Al-Cu Alloys: A Multiscale Analysis Based on First Principles Calculations, *Acta Materialia, 167* (2019), Apr., pp. 121-135
[11] Nayak, S. K., *et al.*, Atomistic Origins of Guinier-Preston Zone Formation and Morphology in Al-Cu and Al-Ag Alloys from First Principles, *Scripta Materialia, 162* (2019), Mar., pp. 235-240
[12] Ravi, C., First-Principles Study of Crystal Structure and Stability of Al?Mg?Si?(Cu) precipitates, *Acta Materialia, 52* (2004), 14, pp. 4213-4227
[13] Xin, J., *et al.*, Prediction of Diffusivities in FCC Phase of the Al-Cu-Mg System: First-Principles Calculations Coupled with CALPHAD Technique, *Computational Materials Science, 90* (2014), July, pp. 32-43
[14] Hu, H., *et al.*, The Structural Stability, Mechanical Properties and Stacking Fault Energy of Al_3Zr Precipitates in Al-Cu-Zr Alloys: HRTEM Observations and First-Principles Calculations, *Journal of Alloys and Compounds, 681* (2016), Oct., pp. 96-108
[15] Kim, K., *et al.*, First-Principles Study of Crystal Structure and Stability of T1 Precipitates in Al-Li-Cu Alloys, *Acta Materialia, 145* (2018), Feb., pp. 337-346

[16] Yang, Q., *et al.*, Suppressing Heating Rate-Dependent Martensitic Stabilization in Ductile Cu-Al-Mn Shape Memory Alloys by Ni Addition: An Experimental and First-Principles Study, *Materials Characterization, 145* (2018), Nov., pp. 381-388
[17] Liu, Y., *et al.*, Understanding Grain Refinement of Sc Addition in a Zr Containing Al-Zn-Mg-Cu Aluminum Alloy from Experiments and First-Principles, *Intermetallics, 123* (2020), 106823
[18] Na, B., *et al.*, First-Principles Calculations of Bulk and Interfacial Thermodynamic Properties of the T1 Phase in Al-Cu-Li Alloys, *Scripta Materialia, 202* (2021), 114009
[19] Chen, X., *et al.*, Data on Atomic Structures of Precipitates in an Al-Mg-Cu Alloy Studied by High Resolution Transmission Electron Microscopy and First-Principles Calculations, *Data Brief, 34* (2021), 106748
[20] Guo, Y., *et al.*, First-Principles Study on Stability, Electronic, Mechanical and Thermodynamic Properties of Al-Cu-RE Ternary Compounds, *Solid State Communications, 287* (2019), Jan., pp. 63-67
[21] Iwaoka, H., Hirosawa, S., First-Principles Calculation of Elastic Properties of Cu-Zn Intermetallic Compounds for Improving the Stiffness of Aluminum Alloys, *Computational Materials Science, 174* (2020), 109479
[22] Zhang, C., *et al.*, Composition Optimization for Al-Zn-Mg-Cu Alloys Based on Thermodynamics and First-Principles Calculations, *Computational and Theoretical Chemistry, 1201* (2021), 113293
[23] Wu, Z., *et al.*, Crystal Structures and Elastic Properties of Superhard IrN_2 and IrN_3 from First Principles, *Physical Review B, 76* (2007), 054115(1)-054115(15)
[24] Mouhao, F., Coudert, F., Necessary and Sufficient Elastic Stability Conditions in Various Crystal Systems, *Physical Review B, 90* (2014), 224104
[25] Li, C. M., *et al.*, First-Principles Calculations of Elastic and Thermodynamic Properties of the Four Main Intermetallic Phases in Al-Zn-Mg-Cu Alloys, *Computational Materials Science, 93* (2014), Oct., pp. 210-220
[26] Li, H., *et al.*, First-Principle Calculations of Structural, Elastic and Thermodynamic Properties of Fe-B Compounds, *Intermetallics*, *46* (2014), Mar., pp. 211-221
[27] Zhou, X., *et al.*, Mechanical Properties and Electronic Structure of Anti-ReO_3 Structured Cubic Nitrides, M_3N, of d Block Transition Metals M: An Ab Initio Study, *Journal of Alloys and Compounds, 595* (2014), May, pp. 80-86
[28] Shao, P., *et al.*, Structural, Electronic and Elastic Properties of the Shape Memory Alloy NbRu: First-Principle Investigations, *Journal of Alloys and Compounds*, *695* (2017), Feb., pp. 3024-3029
[29] Chen, G. Y., *et al.*, First Principles Study of Calcium-Based Sulfur Fixers and Their Products, *Thermal Science*, *26* (2022), 5, pp. 3843-3857
[30] Sun, K., *et al.*, Pt Modified Ultrafine WO_3 Nanofibers: A Combined First-Principles and Experimental Study, *Materials Letters, 236* (2019), Feb., pp. 267-270
[31] Ali, M., *et al.*, Double Bubble Electrospinning: Patents and Nanoscale Interface, *Recent Patents on Nanotechnology, 19* (2024), 3, pp. 453-465
[32] Ali, M., *et al.*, Bipolymer Nanofibers: Engineering Nanoscale Interface via Bubble Electrospinning, *Journal of Applied Polymer Science*, *141* (2023), 5, e54878
[33] Liu, H. Y., *et al.*, Interaction of Multiple Jets in Bubble Electrospinning, *Thermal Science, 27* (2023), 3A, pp. 1741-1746
[34] Li, Y., *et al.*, Fabrication and Characterization of ZrO_2 Nanofibers by Critical Bubble Electrospinning for High-Temperature-Resistant Adsorption and Separation, *Adsorption Science & Technology, 37* (2019), 5-6, pp. 425-437
[35] Sun, J., *et al.*, Rational Design of Electrospun Nanofibers for Gas Purification: Principles, Opportunities, and Challenges, *Chemical Engineering Journal*, *446* (2022), Part 1, 137099
[36] Qian, M. Y., *et al.*, Enhanced Piezoelectric Performance of PVDF Nanofibers by Biomimicking the Spider's Long Liquid Transport, *Chemical Engineering Journal*, *483* (2024), 149159

Paper submitted: December 12, 2023
Paper revised: May 12, 2024
Paper accepted: May 12, 2024